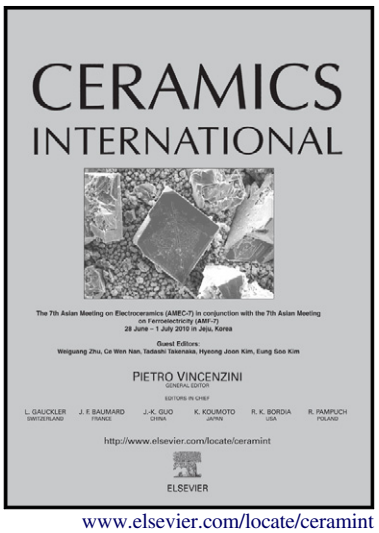

www.elsevier.com/locate/ceramint

Graphene/titanium carbide composites prepared by sol-gel infiltration and spark plasma sintering

Xiaojing Wang, Mingyuan Lu, Ling Qiu, Han Huang, Dan Li, Huanting Wang, Yi-Bing Cheng

PII: S0272-8842(15)01542-4
DOI: http://dx.doi.org/10.1016/j.ceramint.2015.08.017
Reference: CERI11114

To appear in: *Ceramics International*

Received date: 4 June 2015
Revised date: 4 August 2015
Accepted date: 4 August 2015

Cite this article as: Xiaojing Wang, Mingyuan Lu, Ling Qiu, Han Huang, Dan Li, Huanting Wang, Yi-Bing Cheng, Graphene/titanium carbide composites prepared by sol-gel infiltration and spark plasma sintering, *Ceramics International,* http://dx.doi.org/10.1016/j.ceramint.2015.08.017

Graphene/Titanium Carbide Composites Prepared by Sol-Gel Infiltration and Spark Plasma Sintering

Xiaojing Wang,[‡] Mingyuan Lu,[§] Ling Qiu,[‡] Han Huang,[§] Dan Li,[‡] Huanting Wang,[¶] and Yi-Bing Cheng[‡,†]

[‡]Department of Materials Science and Engineering, Monash University, VIC 3800, Australia

[§]School of Mechanical and Mining Engineering, The University of Queensland, QLD 4072, Australia

[¶]Department of Chemical Engineering, Monash University, VIC 3800, Australia

[†]Author to whom correspondence should be addressed. e-mail: yibing.cheng@monash.edu

Abstract

Graphene/titanium carbide composites were synthesized by means of sol-gel infiltration and spark plasma sintering (SPS). The graphene used in this research was casted into a sponge-like shape, composed of a three-dimensional (3D) network of graphene sheets. The sol-gel infiltration synthesis method allowed the formation of nanostructured ceramics inside the porous structure of

graphene networks, thus forming composites. The compositions and microstructures of the Ti-O-C composites changed with the amount of the polymerizable carbon source (i.e. furfuryl alcohol (FA)) in the solution. A high carbon ratio was required to maintain the structure of the graphene network, as the graphene sheets could become a carbon source to react with TiO_2 resulting in a lamellar-shaped grain morphology. Samples after SPS showed some toughening effects, such as de-bonding, bridging and formation of microcracks. Vickers hardness, electrical resistivity and thermal conductivity were examined for the composites.

Keywords: ceramic matrix composites, sol-gel, spark plasma sintering, titanium carbide, nanocomposites

1. Introduction

Titanium carbide (TiC) is an ultra-high temperature ceramic (UHTC), with a low density (4.93 g/cm^3), high melting point (3067 °C), high Vickers hardness (28-35 GPa), high Young's modulus (410-450 GPa), low thermal expansion and high electrical and thermal conductivity.[1,2] Attributed to these characteristics, TiC has been extensively investigated for many applications, including cutting tools, refractory components, electronic elements, aerospace engineering and so on.[2,3] In the last few years, ceramic/carbon composites have attracted tremendous attention from researchers due to their excellent mechanical and functional properties compared with the monolithic counterparts.[4-7]

Carbon nanotubes (CNTs) and carbon fibers are often used in the manufacturing of ceramic composites.[5-7] Recently, the interest in the application of another form of carbon, graphene, is increasing due to its extraordinary mechanical, electrical and thermal properties.[8] The addition of graphene in different ceramics has been investigated.[9-12] Dusza *et al.* reported a Si_3N_4-grpaphene platelet (GPL) composite with improved fracture toughness; the presence of GPLs played an important role in the toughness enhancement by introducing crack deflection, branching and bridging.[9] Ramirez *et al.* reported GPL/Si_3N_4 composites had improved electrical conductivity.[10] Similar studies have been done for other graphene reinforced composites, such as GPL/Al_2O_3.[11,12] However, to the best of our knowledge, there is few study so far investigating the formation and properties of carbide/graphene composites.

Furthermore, the carbon material used in this work is a there-dimensional (3D) graphene network, like a sponge, instead of the traditional two-dimensional (2D) graphene nanosheets. This continuous 3D network is composed of multi-layer graphene sheets and has a cork-like hierarchical structure (Fig. 1). This material is fabricated through thermal reduction of freeze

casted graphene oxide (GO) and exhibits low density, high porosity, and good electrical conductivity and energy absorption efficiency.[13-16] These extraordinary properties promise a wide range of applications of the material, such as electrodes and sensors.[16,17] But in this paper we report its application in the fabrication of ultra high temperature ceramic (UHTC) composites.

In order to fabricate ceramic composites using this 3D graphene network, traditional powder metallurgy approach is not practical, because powders have difficulty to gain full access to the micro-sized pores of the graphene network. Therefore, a sol-gel technique was applied in this study. TiC was synthesized by direct carbothermal reduction of titanium-oxygen-carbon (Ti-O-C) precursors. The Ti-O-C precursor is a sol-gel mixture of titanium alkoxide and furfuryl alcohol (FA), which is as the carbon source.[18-20]

In the present work, novel graphene/TiC composites featuring uniformly distributed graphene sheets and fine TiC grains (the grain size was less than 100 nm) were synthesized. This composite material showed improved toughness and generous energy absorption upon (low-velocity) impact.

2. Experimental Procedure

2.1 Chemicals and synthesis

To synthesis the Ti-O-C precursor, the sol-gel process started with the poly(ethylene oxide)-b-poly(propylene oxide)-b-poly(ethylene oxide) copolymer Pluronic P123 ($EO_{20}PO_{70}EO_{20}$, M_n ~ 5800; Sigma-Adrich). P123 (4.64 g) was dissolved into absolute ethanol (C_2H_5OH, 99.7%) (6.9 g) to form a solution under continuous stirring, to which titanium tetraisopropoxide (TTIP, $Ti(OCH(CH_3)_2)_4$, 97%; Sigma-Adrich) (11.368 g) was added as the titania source. Meanwhile, another solution was prepared by mixing with hydrochloric acid (HCl,

10M) (2.0 g) and absolute ethanol (2.3 g). The acid solution was then added dropwise into the first solution containing TTIP under vigorous magnetic stirring. After half hour, furfuryl alcohol (FA, $C_5H_6O_2$, 98%; Sigma-Adrich) was added into the mixed solution as a carbon source under stirring. Different amounts of FA were added to control the molar ratio of C/Ti in the solutions from 0 to 9. The C/Ti ratio in each composition was calculated based on the amount of FA without consideration of graphene. The solutions were aged for 3 days at the ambient temperature around 25 °C. During the whole process, the continuous stirring was necessary and all the bottles were sealed immediately after mixing. The color of the solution changed from transparent to brown after mixing with FA and then turned to dark brown after 6 hours ageing, indicating the polymerization of FA.

To synthesis the composite precursor, the prepared solution above was then infiltrated into graphene network cells (~ 5 mg/ml) until all the cells were saturated. After that, the solution infiltrated graphene were dried in an oven at 80 °C until the solution becoming a gel. The dried gel was heated to 550 °C at 5 °C/min for 5 hours under nitrogen in order to achieve a mesoporous Ti, O, C matrix with graphene sheets surrounded through pyrolysis of organic components, and then the precursor was infiltrated with the prepared solution again followed by the next steps, and three cycles were applied. Then the samples were further heated to 1450 °C at 2 °C/min for 5 hours under argon for carbothermal reduction to form TiC based graphene composites. The synthesized composites are denoted as G-xC, and referenced TiC are denoted as xC where x indicated the C/Ti ratio in the sol-gel. For example, G-3.8C means sol-gel with C/Ti ratio of 3.8 infiltrated graphene composites, while 3.8C means TiC synthesized from sol-gel with C/Ti ratio of 3.8C. After calcinations, all the samples were crashed and sintered at 1800 °C for 5

min using SPS, at a maximum heating rate of 200 °C/min under vacuum and a pressure of 40 MPa.

2.2 Characterization

Several characterization methods were used to examine the samples. X-ray diffraction (XRD) patterns were recorded from 10° to 80° of the 2θ values, using a step size of 0.02° and a scan rate of 2°/min, through a Philips PW1140/90 diffractometer operated with CuK_{α} radiation at 40 kV and 25 mA. The thermogravimetric analyzer (Perkin-Elmer, Pyris 1) was conducted in air to 800 °C at a heating rate of 5 °C/min to obtain the thermogravimetric analyses (TGA) graphs. Raman spectra were recorded on a RenishawinVia Raman Microscope with a 514 nm argon ion laser at room temperature. A JEOL 7001F microscope operated at 15 kV and FEI Tecnai T20 operated at 200 kV microscope were employed to take scanning electron microscope (SEM) and transmission electron microscope (TEM) images respectively. All the microscopes were equipped with EDS for qualitative chemical analysis. The SEM samples were prepared by cutting and polishing. The TEM samples were prepared by grinding powders under *n*-butanol in a mortar and placing a drop of the suspension on a holey-carbon grid. Density of the sintered samples was measured using a liquid displacement method, Archimedes' technique. Vickers indentation (Duramin A-300 hardness tester) was used to measure the fracture toughness K_{1C} of the specimens; the applied load was 5kgf and Shetty equation[21] was used to calculate K_{1C}. Nanoindentation test was performed at room temperature on a TI900 Hysitron Triboindenter to measure the hardness (H) and elastic modulus (E) of the samples. The load applied was 100 mN and the load function used involves 10s loading to the maximum load, 5s holding at the maximum load and 15s unloading. At least 10 indents were repeated on different locations of a specimen.

3. Results and Discussion

3.1 Effect of the C/Ti ratio in the precursor compositions

3.1.1 Compositions with different C/Ti ratios

The compositions of the samples after 1450 ºC treatment with different C/Ti ratios were analyzed by XRD patterns, TGA curves and Raman spectrums. Fig. 2 shows the XRD results of the samples after 1450 ºC treatment with C/Ti ratios varying from 0 to 9. TiC is the major phase identified in the XRD patterns for samples with C/Ti ratios over 3.8. A small mount of impurities was detected (e.g. peak around 45º for sample G-6C), but was unable to be identified. The volume of the impurities was too small to be detected by the EDS. Ti and C are the elements identified by EDS. However, for the samples with C/Ti ratios less than 3, both TiC and Ti_2O_3 phases are present.

Theoretically, a carbon to titanium (C/Ti) ratio of 3 is able to fully convert TiO_2 to TiC based on the chemical equilibrium.[22] However, due to the evaporation of FA during the initial sol-gel process and PFA during drying and calcination processes, a designed C/Ti ratio of 3 in the composition was found not sufficient to complete the carbothermal reaction. A complete oxidation of TiC to TiO_2 would result in a weight gain of 33.3%.[23] Based on the TGA results (Fig. 3), the sample with C/Ti ratio of 3.8 shows a weight gain around 33.3% above ~400 ºC, while samples with smaller C/Ti ratios show less weight gains and samples with larger C/Ti ratios show a weight loss after the initial weight gain at a higher temperature due to the oxidation of excessive carbon in the compositions. The TGA results indicated that 3.8 was the minimum C/Ti ratio for a full conversion of TiO_2 to TiC in this work. The TGA results are consistent with the XRD analysis.

The formation of TiC and Ti_2O_3 in the samples with zero C/Ti ratio indicated that graphene could react with TiO_2 as a carbon source, which is also proven by its weight gain observed in the TGA curve. However, the amount of graphene was not sufficient for a complete reduction, so some partially reduced oxide, Ti_2O_3 formed as an intermediate product of carbothermal reduction. Even for the sample with a C/Ti ratio of 3, there was still a carbon shortage, which indicated that the amount of carbon derived from graphene was tiny.

The status of carbon in the composites was investigated by Raman spectroscopy. Fig. 4 shows two peaks, at ~1350 and ~1600 cm^{-1}, referred as D and G peaks in all the samples. Both D and G peaks are related to vibrations of sp^2-hybridized carbon bonds. Their positions, shape, and the I_D/I_G intensity ratio provide information about the degree of order in the carbon network.[23,24] The 2D peak, the overtone of D peak, is normally used to identify the monolayer graphene when it is sharp and high, appearing broadly at ~2670 cm^{-1}. The combination mode (D+D′) at ~2930 cm^{-1} is defect activated.[25,26] The Raman spectrums (Fig. 4) proved the presence of graphene in the samples after firing at 1450 ºC with C/Ti ratios of 6 and 9, in which carbon derived from PFA was more than enough for a complete carbothermal reduction. The increased ratio of I_D/I_G in samples with a C/Ti ratio of 6 and 9 compared with pure graphene network indicated an increased ordering of carbon in the composites. [23,24]

3.1.2 Microstructures with different C/Ti ratios in the precursors

The microstructures of the samples with different C/Ti ratios after 1450 ºC treatment are shown in Fig. 5. Graphene sheets can be observed in samples with a C/Ti ratio higher than 3.8. The higher the C/Ti ratio, the more graphene sheets can be remained in the final composites, based on the SEM analysis. The sample with a C/Ti ratio of 9 had lots of graphene sheets

uniformly distributed in the matrix, but in the sample with a C/Ti ratio of 3.8, there were only a few of thin graphene sheets in the sample. No graphene sheets can be found in the samples with a C/Ti ratio less than 3. It is difficult to say which form of carbon, between the carbon from the decomposed polymer and the graphene, is more reactive in this case. However, the carbon derived from PFA is able to uniformly distributed around every TiO_2 particle because of the polymerization of FA forming a homogenous network (Fig. 5(f)), so that it would be more easily for TiO_2 particles to react with the carbon derived from PFA. For the samples with an insufficient amount of PFA derived carbon, TiO_2 grains near graphene sheets would react with the graphene for carbothermal reduction, forming TiC or partially reduced Ti_2O_3 according to the XRD results.

The grains also changed with different amounts of C/Ti ratio in the samples. Samples with a higher C/Ti ratio had a smaller grain size. In the samples with C/Ti ratio of 3.8, 6 and 9, there was only the TiC phase and the grain size was around 50 to 100 nm. The carbon derived from PFA can restrict grain growth of TiC, as it can form a uniform network around each grain. Our previous work also proved that after 1450 ºC firing, the amorphous carbon derived from PFA can form several graphene-type layers on the surface of TiC grains, which could retard the grain growth as well as densification.[27] The grain size was not uniform for samples with a low C/Ti ratio. A bi-model distribution of grains existed, where some grains remained in a nano scale and some were coarsened to several microns (Fig. 5 (a, b)). As these samples contained TiC and Ti_2O_3 phases according to XRD results, it was possible that graphene was involved in the carbothermal reduction as a carbon source for reducing the contacted TiO_2 grains. As graphene had a sheet structure, it templated the grain growth of the reduced product of TiO_2, i.e. TiC or Ti_2O_3, forming coarsened grains.

This template effect was more obvious in the sample with zero FA, where the only carbon source was the graphene sponge. Some lamellar/plate-shaped TiC and reduced titanium oxides are observed (Fig. 6), which is very different from the conventional particle-shaped TiC or titanium oxides. This microstructure is clearly associated with the intrinsic lamellar structure of grapheme. No further investigation was done on this aspect, as it is beyond the scope of this research.

3.2 Microstructures and properties of the densified composites

Three compositions with a C/Ti ratio of 3.8, 6 and 9 respectively were sintered at 1800 ºC for 5 minutes under 40MPa, after carbothermal reduction at 1450 ºC for 5 hours. The XRD results proved that TiC and carbon were present in the samples after SPS (Fig. 7). The peak intensities for the impurities were weakened compared with the XRD patterns of the samples after carbothermal reduction, which could be a result of more complete reaction due to high temperature SPS sintering. SEM images of the polished surfaces of the samples after SPS are shown in Fig. 8. According to the SEM images, the sample with a C/Ti ratio of 3.8 showed a different microstructure compared with that having a higher C/Ti ratio.

The SPS sintered sample with 3.8 C/Ti had larger grains around 1 μm, and showed no obvious sign of the presence of the graphene network. In a high magnification image (Fig. 8(b)), some individual thin and small graphene sheets can be observed from the surface pores. The SPS sintered samples with a C/Ti ratio of 6 and 9 showed interesting microstructures of a very fine TiC grain matrix is dispersed by a uniform carbon network derived from graphene (Fig. 8(c, e)). The grain size of TiC remains around 100 nm even after the high temperature sintering, so no obvious grain growth happened during sintering, which may be restricted by the excessive carbon in the compositions.

A bi-model distribution of the grain size is also observed in these SPS sintered samples. Two different sizes of TiC grains were observed in each sample (Fig. 8(b, d, f)). This phenomenon may happen due to the fact that in the system, there were two different kinds of carbon sources; carbon derived from PFA and graphene network. As what has discussed above, graphene sheets was able to template the grain growth of TiC to form coarsened grains. Another reason is that some grains especially from the surface during the infiltration may not undertake restricted force from graphene network, which facilitates grain growth for these grains.

Fig. 9 shows the effect of the C/Ti ratio on the porosity and density. It is clearly seen that a higher C/Ti ratio resulted in higher apparent porosity and lower density. The amorphous carbon derived from PFA has a relatively low density (1.8-2.1 g/cm^3) and the carbon is very difficult to be densified.[28] The specimens with a higher C/Ti ratio are enriched with carbon and thus have lower density and higher porosity. The Young's modulus *E* and hardness *H* values measured using the nanoindentation are summarized in Table 1. Both *E* and *H* decrease with the increase of the C/Ti ratio. The decrease in *E* and *H* is likely attributed to the increase of the soft amorphous carbon derived from PFA and porosity.

The composites had quite different properties compared with the reference TiC samples prepared by sol-gel synthesis and SPS under same conditions. The presence of graphene in the composites not only increased the carbon concentration but also limited the densification of the samples, resulting in significantly reduced density and increased porosity, especially for the sample with C/Ti ratio of 6. This also produced much lower hardness and elastic modulus for the graphene added samples compared with the reference sample. This effect appeared not that significant, however, in the samples with lower or higher C/Ti ratios because the overall carbon concentration in these samples was either too low or too high to cause a significant difference

between the reference and the graphene containing samples. Both porosity and preserved graphene influenced the mechanical properties of the samples. Sample G-9C has similar porosity as the reference sample, but shows different hardness and fracture behavior.

3.3 Toughening and its mechanisms

The fracture toughness of the SPS sintered G-3.8C specimen was found to be higher than that of the reference sample, but it is difficult to estimate the fracture toughness for other graphene containing samples with higher C/Ti ratios. The impressions of the Vickers hardness indents on SPS sintered samples G-6C and G-9C were examined using SEM. The SEM micrographs of the fracture patterns show no regular cone and radial/median cracks (Fig. 10 (a, b)) and the indentation-induced cracks are prone to propagate along the graphene sheets and TiC grain boundaries (Fig. 10 (c, d)). The fracture behavior of the graphene containing composite does not follow the conventional fracture patterns of brittle ceramics, where four straight cracks emanate from the four corners of the diamond shaped indentation, which is an indication of toughening. However, it is very difficult to quantify the fracture toughness improvement, as the toughness measurement using the Vickers indentation technique requires well-defined fracture pattern.

Based on the images in Fig. 10, the indentation depth is small and there are cracks inside the indents. No obvious cracks were found outside the indentation. Furthermore, most of cracks inside the indents happened along the paths of graphene sheets, resulting in de-bonding of graphene sheets. Some bridging effect by the graphene sheets was observed in the SEM images (Fig. 10 (c, d)).

In the two samples that have high carbon contents, the carbon derived from PFA protected graphene sheets from reaction with TiO_2, resulting in a structure of fine TiC grains

surrounded by the graphene network. In this structure, the graphene sheets acted as a weak phase. The wall of the network is consisted of several layers of graphene sheets. Even though there was enough carbon derived from PFA for carbothermal reduction, the TiO_2 grains attached on the surface of the graphene wall could also react with graphene to form TiC, resulting in a strong interface between the surface of the graphene wall and the TiC matrix after SPS densification. During crack propagation under the indenter, peelings of graphene sheets would occur at the surface and the internal of the graphene wall due to weak van der Waals bonding between the graphene sheets. The peelings between graphene sheets create lots of new surface areas to absorb fracture energy, thus toughen the composites. Bridging is another toughening mechanism in the composites (Fig. 10 (c, d)). In this mechanism, the graphene sheets acted as bridges to connect both sides of cracks and induced some sort of crack closure. The de-bonding of graphene sheets and bridging by graphene were also observed in the fracture surfaces (Fig. 10 (e, f)).

The peeling of graphene sheets in the graphene walls is proven to be an energy comsuming process. The indentation load-displacement curves (*P-h* curves) shown in Fig. 11 give insight into this energy absorption effect. The net area enclosed by the *P-h* curve represents the work done on the system and is manifested as plastic deformation as well as elastic energy stored within the specimen.[29,30] For the graphene/TiC samples, the 'fat belly' of the *P-h* curves indictes that the composites absorbed some strain energy during loading of stress, while at the same time exhibited some elastic recovery upon unloading.[30] This effect was more obvious for G-6C sample because the energy absorption was associated with both increased porosity and preserved graphene. For G-3.8C and G-9C samples, the energy absorption effect became less significant due to either limited graphene preserved or too much residual carbon resulting high porosity.

4. Conclusions

Graphene/TiC composites have been successfully synthesized using a sol-gel infiltration into a novel graphene sponge and spark plasma sintering. Furfurly alcohol (FA) was employed as a carbon source. From the carbothermal reduction point of view, the FA was a more desirable carbon source than the graphene sheets in the sponge as the polymerized FA formed a uniform carbon network around each TiO_2 particle. However, if the amount of PFA was insufficient for a complete carbothermal reduction, the graphene sheets would react with TiO_2 as a carbon source. In order to maintain a graphene network in the sample, a high C/Ti ratio is preferred. The lamellar shape of the graphene sheets had a template effect on the grain growth of TiC or reduced titanium oxide when acting as a carbon source, forming a lamellar shape of ceramic grains after 1450 ºC heat treatment. The SPS sintered samples with a C/Ti ratio of 6 to 9 showed an interesting microstructure of fine TiC grains surrounded by a graphene network. On the other hand, higher C/Ti ratios resulted in lower density and poorer hardness due to the extra carbon in the samples. The graphene network in the sample can toughen the materials by peeling of the graphene walls and crack bridging, and the composites also showed a potential for shock/impact absorption under indentation.

Acknowledgements

X. Wang acknowledges a scholarship from the Monash University. The authors acknowledge the use of facilities within the Monash Centre for Electron Microscopy (MCEM).

References

[1]H.H. Hwu and J.G. Chen, "Surface chemistry of transition metal carbides", *Chem. Rev.*, **105**, 185-212 (2005).

[2]H.O. Pierson, *Handbook of Refractory Carbides and Nitrides* , William Andrew Publishing/Noyes, 1996.

[3]S.T. Bae, H. Shin, H.S. Jung and K.S. Hong, "Synthesis of Titanium Carbide Nanoparticles with a High Sepcific Surface Area from a TiO_2 Core-Sucrose Shell Precursor", *J. Am. Ceram. Soc.*, **92**, 2512-2516 (2009).

[4]B.P. Tarasov, V.E. Muradyan, and A.A. Volodin, "Synthesis, properties, and examples of the use of carbon nanomaterials", *Russ. Chem. Bull.*, **60**, 1261-1273 (2011).

[5]A. Sayir, "Carbon fiber reinforced hafnium carbide composite", *J. Mater. Sci.*, **39**, 5995-6003 (2004).

[6]G.L. Hwang and K.C. Hwang, "Carbon nanotube reinforced ceramics", *J. Mater. Chem.*, **11**, 1722-1725 (2001).

[7]Y.M. Zhang, S. Li, J.C. Han, and Y.F. Zhou, "Fabrication and characterization of random chopped fiber reinforced reaction bonded silicon carbide composite", *Ceram. Int.*, **38**, 1261-1266 (2012).

[8]A.K. Geim, K.S. Novoselov, "The rise of graphene", *Nat. Mater.*, **6**, 183-191 (2007).

[9]J. Dusza, J. Morgiel, A. Duszová, L. Kvetková, M. Nosko, P. Kun, and C. Balázsi, "Microstructure and fracture toughness of Si3N4 + graphene platelet composites", *J. Eur. Ceram. Soc.*, **32**, 3389-3397 (2012).

[10]C. Ramirez, F.M. Figueiredo, P. Miranzo, P. Poza, and M.I. Osendi, "Graphene nanoplatelet/silicon nitride composites with high electrical conductivity", *Carbon*, **50**, 3607-3615 (2012).

[11]K. Wang, Y. Wang, Z. Fan, J. Yan and T. Wei, "Preparation of graphene nanosheet/alumina composites by spark plasma sintering", *Mater. Res. Bull.*, **46**, 315-318 (2011).

[12]Y. Fan, L. Wang, J. Li, S. Sun, F. Chen, L. Chen and W. Jiang, "Preparation and electrical properties of graphene nanosheet/Al_2O_3 composites", *Carbon*, **48**, 1743-1749 (2010).

[13]L. Qiu, J.Z. Liu, S.L. Chang, Y. Wu and D. Li, "Biomimetic superelastic graphene-based cellular monoliths", *Nat. Commun.*, **3**, 1241-1247 (2012).

[14]F. Liu and T.S. Seo, "A controllable self-assembly method for large-scale synthesis of graphene sponges and free-standing graphene films", *Ad. Funct. Mater.*, **20**, 1930-1936 (2010).

[15]Z. Chen, W. Ren, L. Gao, B. Liu, S. Pei and H.M. Cheng, "Three-dimensional flexible and conductive interconnected graphene networks grown by chemical vapour deposition", *Nat. Mater.*, **10**, 424-428 (2011).

[16]X. Zhang, Z. Sui, B. Xu, S. Yue, Y. Luo, W. Zhan and B. Liu, "Mechanically strong and highly conductive graphene aerogel and its use as electrodes for electrochemical power sources", *J. Mater. Chem.*, **21**, 6494-6497 (2011).

[17]X. Xie, G. Yu, N. Liu, Z. Bao, C. S. Criddle and Y. Cui, "Graphene-sponges as high-performance low-cast anodes for microbial fuel cells", *Energy Environ. Sci.*, **5**, 6862-6866 (2012).

[18]C. Giordano and M. Antonietti, "Synthesis of crystalline metal nitride and metal carbide nanostructures by sol–gel chemistry", *Nano Today*, **6**, 366-380 (2011).

[19]J. Livage and C. Sanchez, "Sol-gel chemistry", *J. Non-Cryst. Solids*, **145**, 11-19 (1992).

[20]J. Zhong, S. Liang, K. Wang, H. Wang, T. Williams, H. Huang, and Y.B. Cheng, "Synthesis of Mesoporous Carbon-Bonded TiC/SiC Composites by Direct Carbothermal Reduction of Sol-Gel Derived Monolithic Precursor, *J. Am. Ceram. Soc.*, **94**, 4025-4031 (2011).

[21]M. Antonov, and F. Sergejev "Comparative study on indentation fracture toughness measurements of cemented carbides", *Proc. Eston. Acad. Sci. Eng.*, **12**, 388-398 (2006).

[22]W. Sen, B.Q. Xu, B. Yang, H.Y. Sun, J.X. Song, H.L. Wan and Y.N. Dai, "Preparation of TiC powders by carbothermal reduction method in vacuum", *Trans. Nonferrous Met. Soc. China*, **21**, 185-190 (2011).

[23]F. Tuinstra and J.L. Koenig, "Raman Spectrum of Graphite," *J. Chem. Phys.*, **53**, 1126-1130 (1970).

[24]M. Nakamizo, "Raman-Spectra of Iron-Containing Glassy Carbons," *Carbon*, **29**, 757–761 (1991).

[25]D.C. Elias, R.R. Nair, T.M.G. Mohiuddin, S.V. Morozov, P. Blake, M.P. Halsall, A.C. Ferrari, D.W. Boukhvalov, M.I. Katsnelson, A.K. Geim, and K.S. Novoselov, "Control of Graphene's Properties by Reversible Hydrogenation: Evidence for Graphane," *Science*, **323**, 610–613 (2009).

[26]A.C. Ferrari, J.C. Meyer, V. Scardaci, C. Casiraghi, M. Lazzeri, F. Mauri, S. Piscanec, D. Jiang, K.S. Novoselov, S. Roth, and A.K. Geim, "Raman Spectrum of Graphene and Graphene Layers," *Phys. Rev. Lett.*, **97**, 187401-187404 (2006).

[27]J. Zhong, S. Liang, K. Wang, H. Wang, T. Williams, H. Huang and Y.B. Cheng, "Synthesis of Mesoporous Carbon-Bonded TiC/SiC Composites by Direct Carbothermal Reduction of Sol-Gel Derived Monolithic Precursor", *J. Am. Ceram. Soc.*, **94**, 4025-4031 (2011).

[28]S.K. Mishra, L.C. Pathak, "Effect of carbon and titanium carbide on sintering behavior of zirconium diboride", *J. Alloys Compd.*, **465**, 547-555 (2008).

[29]C.A. Schuh, Nanoindentation studies of materials, *Mater. Today*, **9**, 32-40 (2006).

[30]W.C. Oliver and G.M. Pharr, An improved technique for determining hardness and elastic modulus using load and displacement sensing indentation experiments, *J. Mater. Res.,* **7**, 1564-1583 (1992).

Graphene/Titanium Carbide Composites Prepared by Sol-Gel Infiltration and Spark Plasma Sintering

Xiaojing Wang,‡ Mingyuan Lu,§ Ling Qiu,‡ Han Huang,§ Dan Li,‡ Huanting Wang,¶ Yi-Bing Cheng‡,†

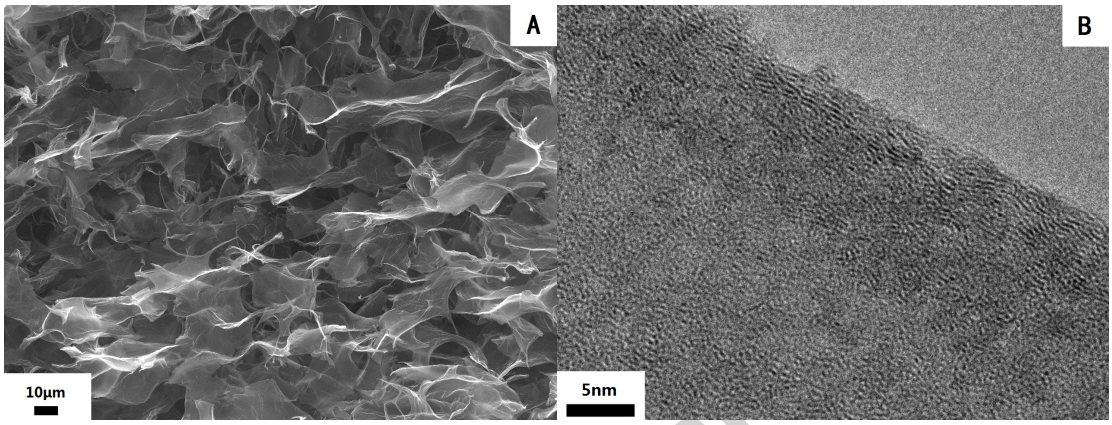

Fig.1 (a) SEM and (b) TEM micrographs of the 3D graphene network.

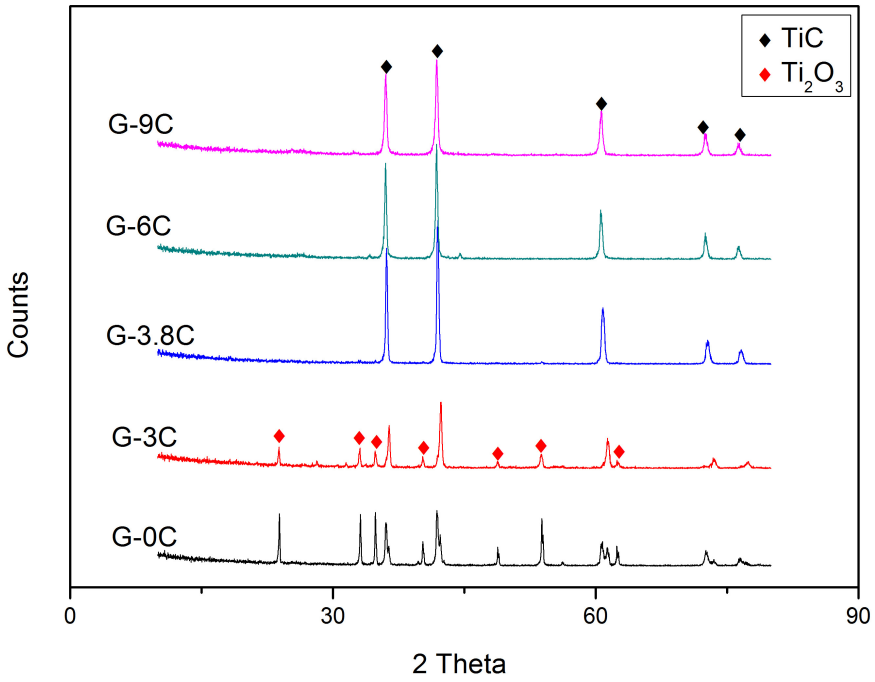

Fig.2 XRD patterns of the sol-gel synthesized Ti-O-C-graphene precursors with different C/Ti ratios after 1450 ºC treatment in Ar for 5 hours. The carbon to Ti ratio, excluding graphene, for each composition is marked in the sample name.

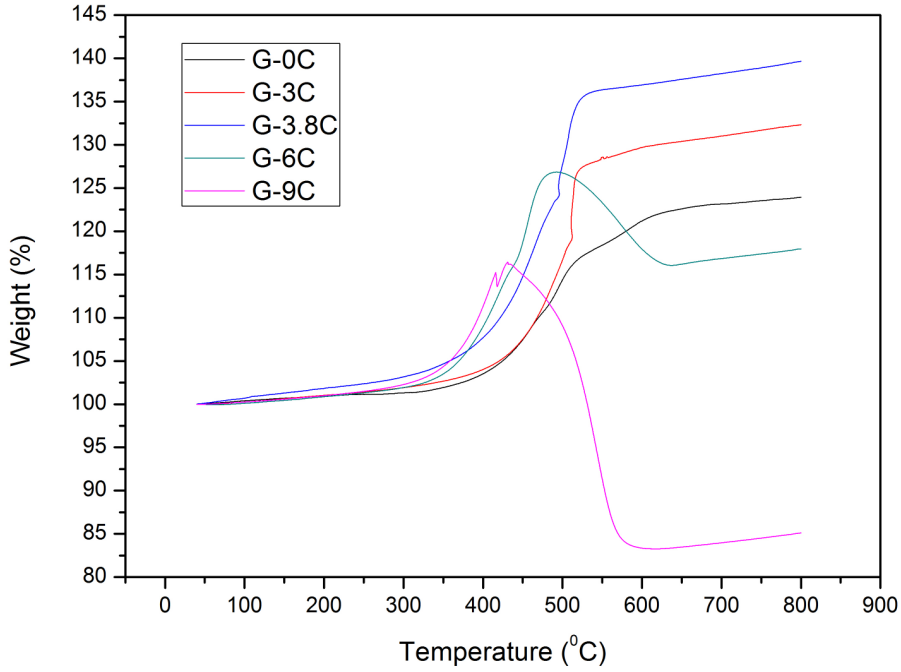

Fig.3 TGA curves of the sol-gel synthesized Ti-O-C-graphene precursors with different C/Ti ratios from 0 to 9 after 1450 ℃ treatment for 5 hours in Ar.

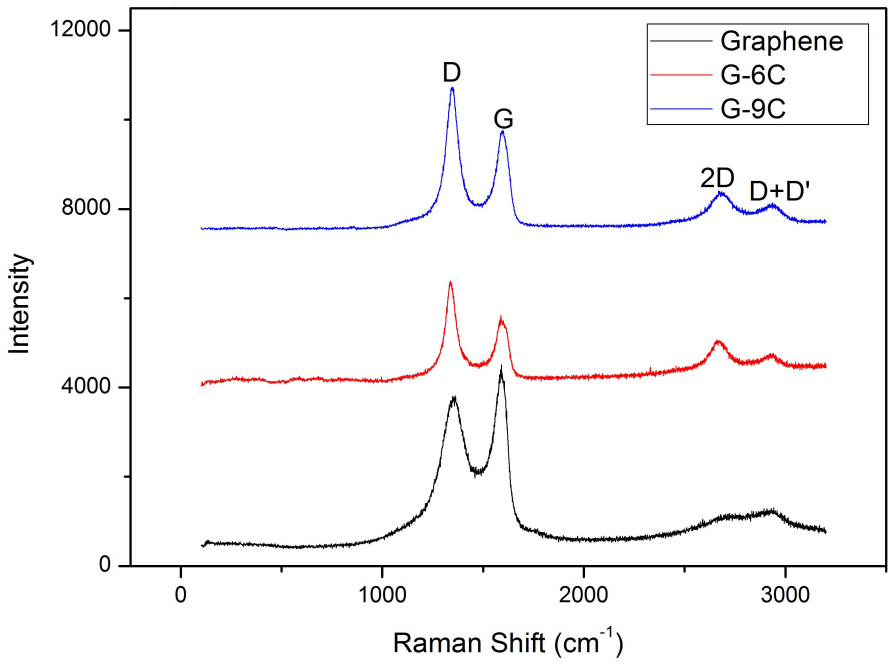

Fig.4 Raman spectra of the graphene; and sol-gel synthesized Ti-O-C-graphene precursors with a C/Ti ratio of 6 and 9 respectively, after 1450 ºC treatment for 5 hours in Ar.

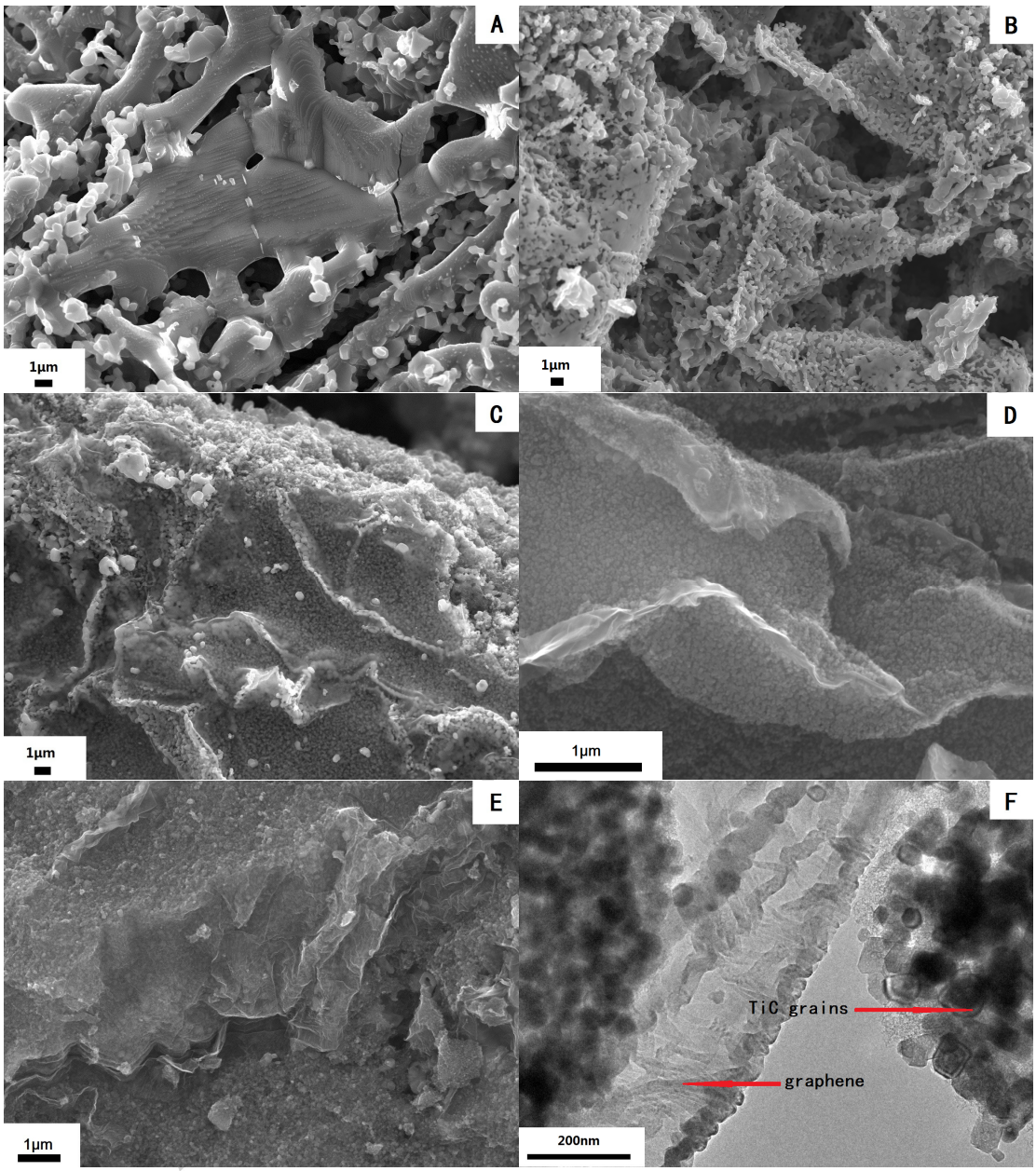

Fig.5 SEM micrographs of sol-gel synthesized Ti-O-C-graphene samples after 1450 ℃ treatment for 5 hours in Ar, with C/Ti ratios of 0 (A), 3 (B), 3.8 (C), 6 (D) and 9 (E), respectively; A TEM image of the matrix of sol-gel synthesized Ti-O-C-graphene precursors with the C/Ti ratio of 9 after 1450 ℃ treatment for 5 hours in Ar (F).

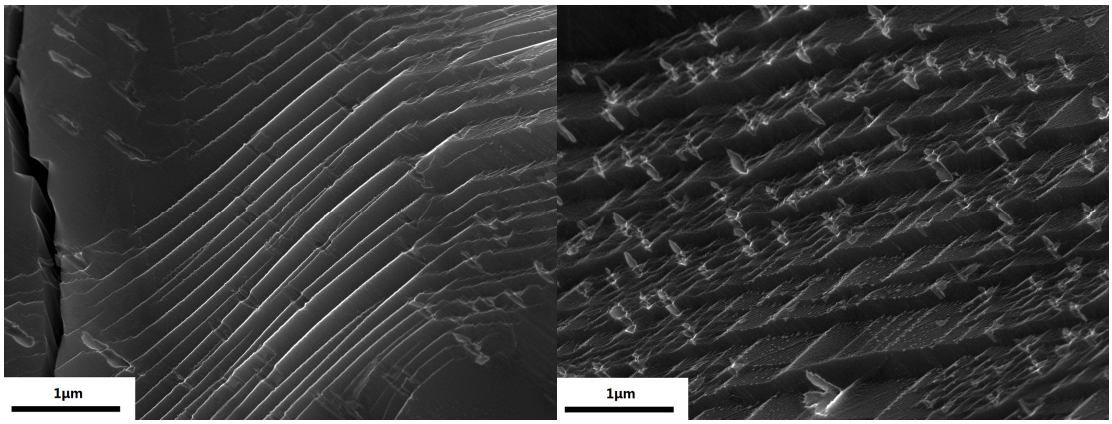

Fig.6 SEM micrographs of the lamellar-shaped structure in the sol-gel synthesized Ti-O-C-graphene precursors with zero FA after 1450 ºC treatment for 5 hours in Ar.

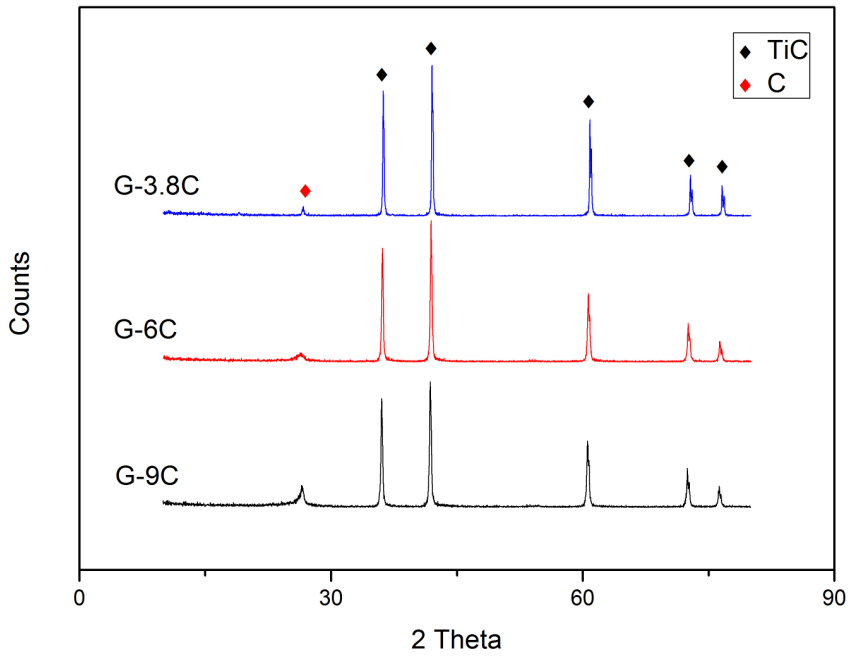

Fig.7 XRD patterns of graphene/TiC composites with a Ti/C ratio of 3.8, 6 and 9 respectively after SPS at 1800 ℃ for 5 min in vacuum.

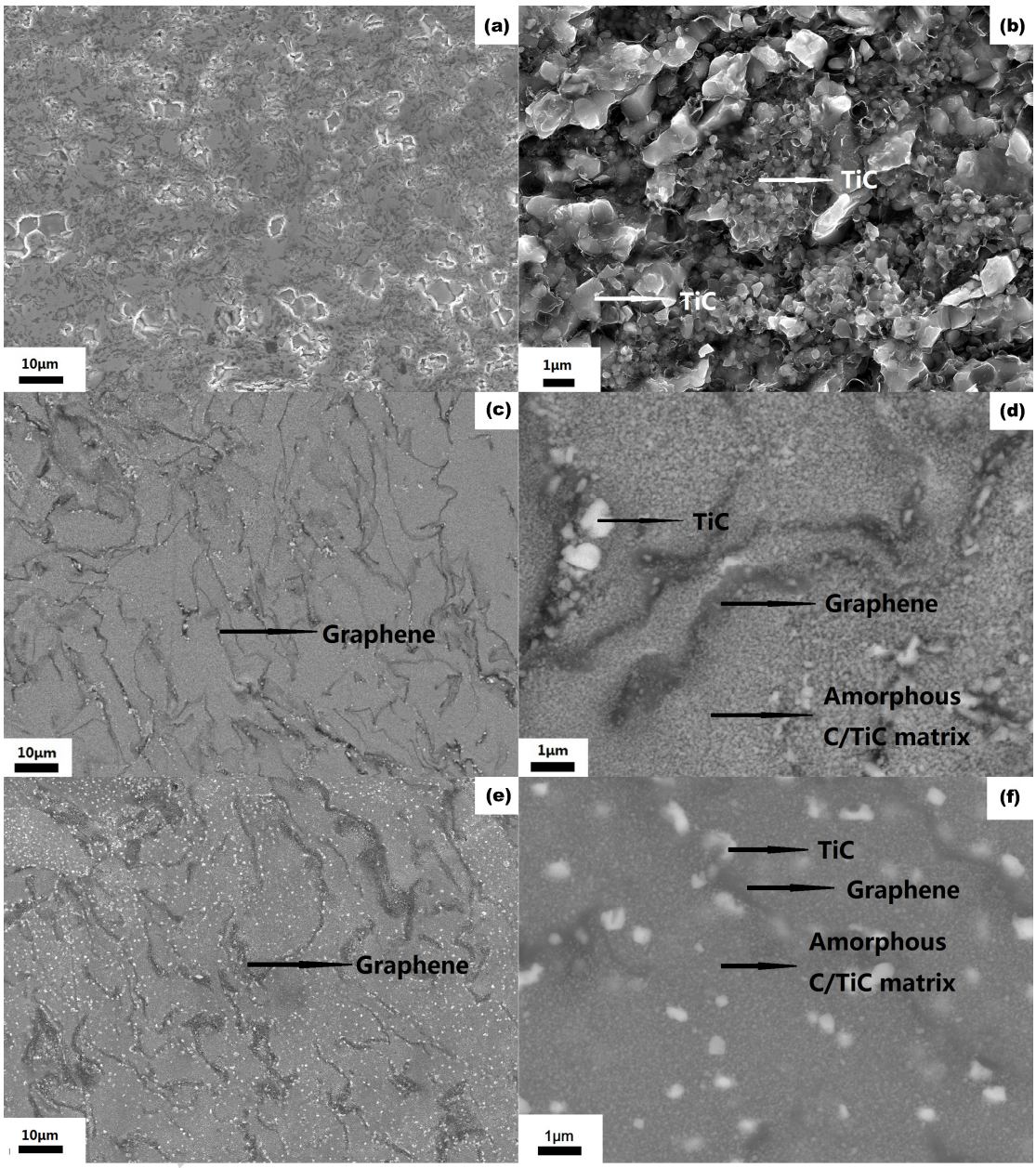

Fig.8 SEM micrographs of graphene/TiC composites with Ti/C ratio of 3.8 (a & b), 6 (d & d) and 9 (e & f) after SPS at 1800 ℃ in vacuum for 5 min. The graphene walls are seen in the high carbon containing samples.

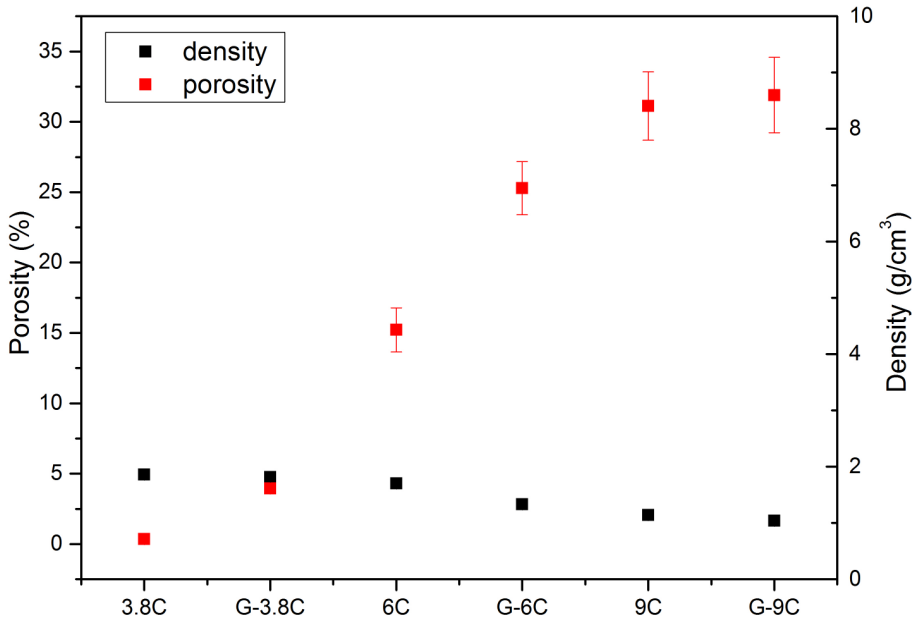

Fig. 9 Variation of density and porosity of SPS sintered graphene/TiC composites and corresponding reference TiC samples with different C/Ti ratios.

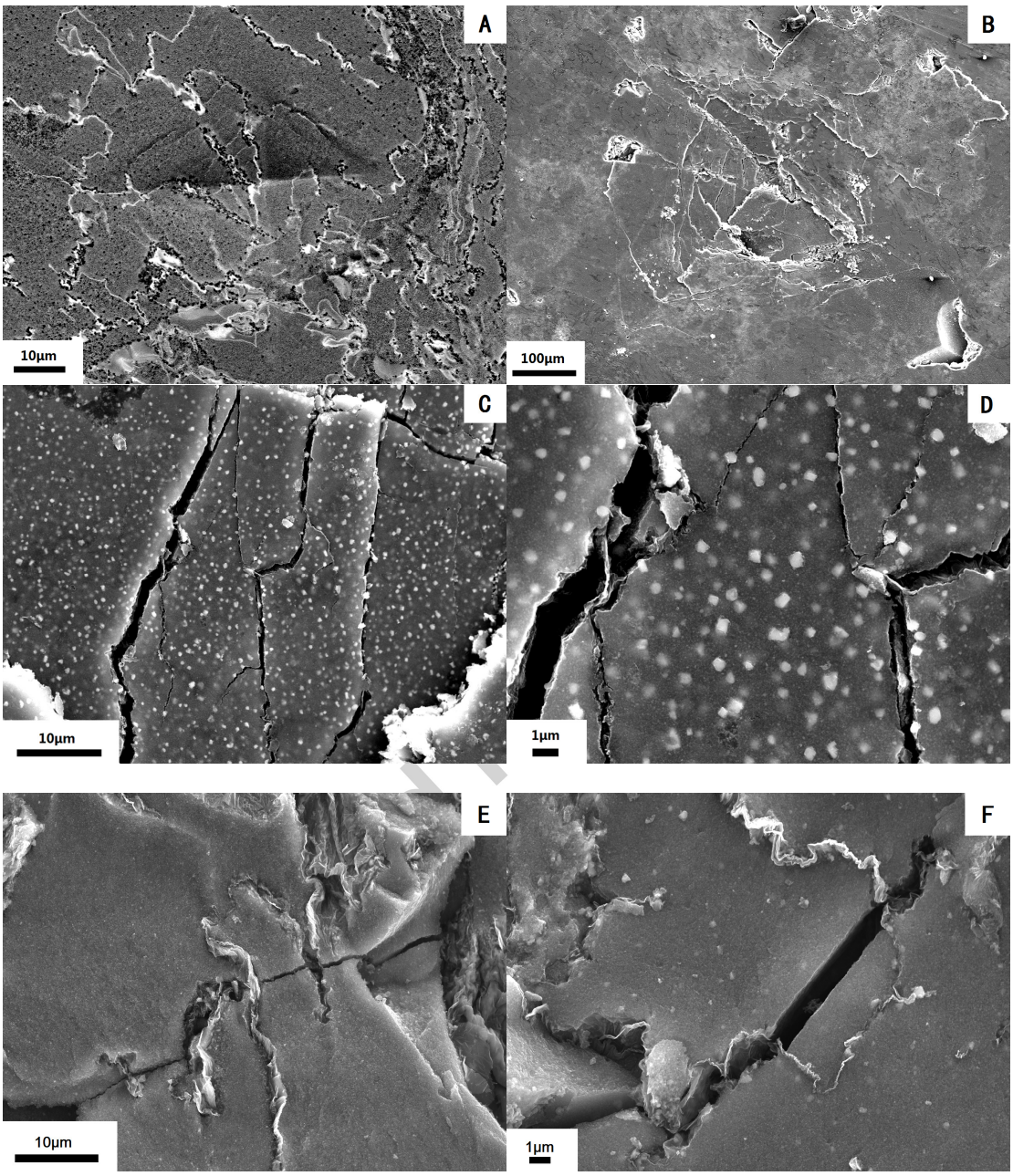

Fig.10 SEM micrographs of Vicker's hardness indentations on the graphene/TiC composite with (A) sample G-6C under a 0.3kgf load; and (B) sample G-9C under a 5kgf load; (C and D) show cracks inside the indentation on the SPSed sample G-9C; (E and F) show fracture surface of SPSed sample G-6C.

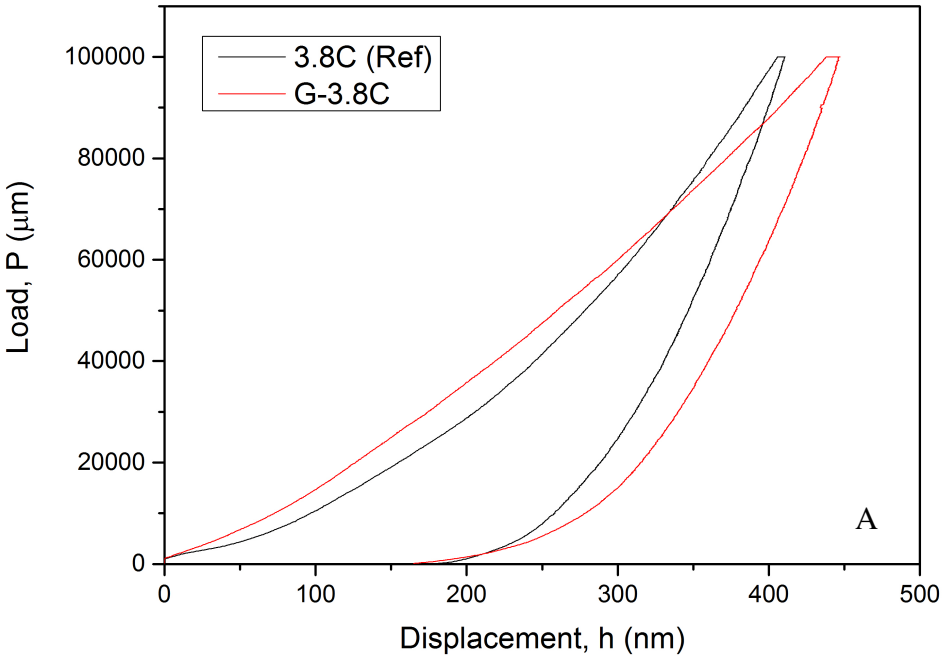

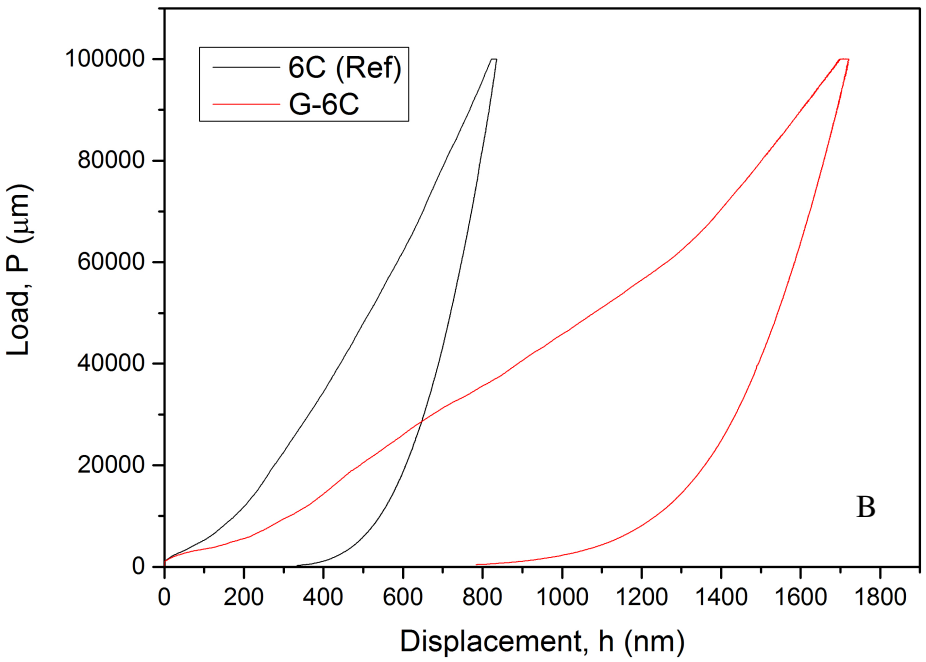

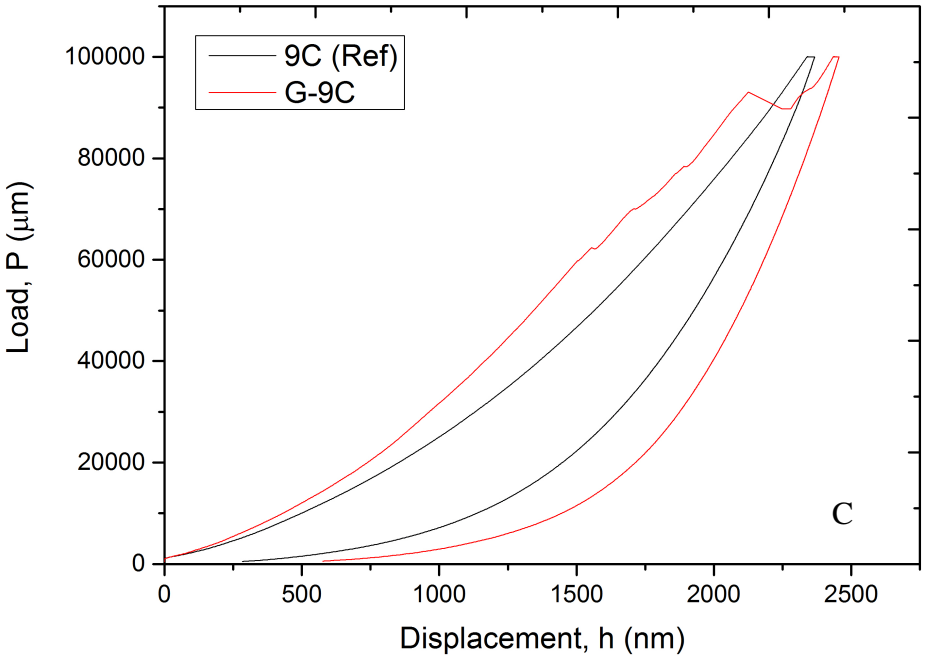

Fig.11 The load-displacement (*P-h*) curves of indentations on graphene/TiC composites with different C/Ti ratios; (A) 3.8C; (B) 6C; (C) 9C. The curves in black lines were those obtained from indentation on the reference samples.

Table 1 Properties of SPS sintered graphene/TiC composites with different C/Ti ratios and reference TiC samples

Samples	Hardness (GPa)	Elastic Modulus (GPa)	Fracture Toughness ($MPa \bullet m^{1/2}$)
3.8C (Ref)	28.49 ± 6.09	408.13 ± 48.49	2.09 ± 0.31
G-3.8C	15.28 ± 4.57	293.27 ± 41.12	2.24 ± 0.33
6C (Ref)	10.08 ± 4.06	191.56 ± 56.21	4.21 ± 0.58
G-6C	1.62 ± 0.45	30.33 ± 9.49	---
9C (Ref)	1.03 ± 0.06	10.99 ± 0.39	4.98 ± 0.64
G-9C	0.85 ± 0.09	11.18 ± 0.56	---